Articles

Estimation of Inter-Residue Distances in Spin Labeled Proteins at Physiological Temperatures: Experimental Strategies and Practical Limitations†

Christian Altenbach,‡ Kyoung-Joon Oh,‡,§ René J. Trabanino,‡ Kálmán Hideg,|| and Wayne L. Hubbell*,‡

Jules Stein Eye Institute and Department of Chemistry and Biochemistry, University of California, Los Angeles, California 90095-7008, and Institute of Organic and Medicinal Chemistry, University of Pécs, H-7643 Pécs, Hungary

Received July 24, 2001; Revised Manuscript Received October 16, 2001

ABSTRACT: Magnetic dipolar interactions between pairs of solvent-exposed nitroxide side chains separated by approximately one to four turns along an α-helix in T4 lysozyme are investigated. The interactions are analyzed both in frozen solution (rigid lattice conditions) and at room temperature as a function of solvent viscosity. At room temperature, a novel side chain with hindered internal motion is used, along with a more commonly employed nitroxide side chain. The results suggest that methods developed for rigid lattice conditions can be used to analyze dipolar interactions between nitroxides even in the presence of motion of the individual spins, provided the rotational correlation time of the interspin vector is sufficiently long. The distribution of distances observed for the various spin pairs is consistent with rotameric equilibria in the nitroxide side chain, as observed in crystal structures. The existence of such distance distributions places important constraints on the interpretation of internitroxide distances in terms of protein structure and structural changes.

Site-directed spin labeling (SDSL)[1] has been established as an important tool for the determination of structure and dynamics in both soluble and membrane proteins of arbitrary molecular weight (see refs *1*−*5* for reviews). In the most common implementation of SDSL, site-directed cysteine mutants are reacted with a methanethiosulfonate nitroxide reagent to produce the side chain designated R1 (Figure 1). Primary quantities determined from the EPR of a single R1 in a protein include the solvent accessibility and mobility of the side chain. The sequence dependence of these quantities serves to identify regular secondary structure and its orientation within the protein.

If two R1 side chains are introduced into a protein, magnetic dipolar interactions between them can be analyzed in terms of interspin distance. Such distance measurements are important in SDSL because they provide global structural constraints which, when taken together with secondary structure, are often sufficient to model a protein at the level of the backbone fold (*6*−*10*). In addition, changes in dipolar interactions can produce large spectral changes, making it particularly straightforward to monitor conformational changes (*11*−*15*).

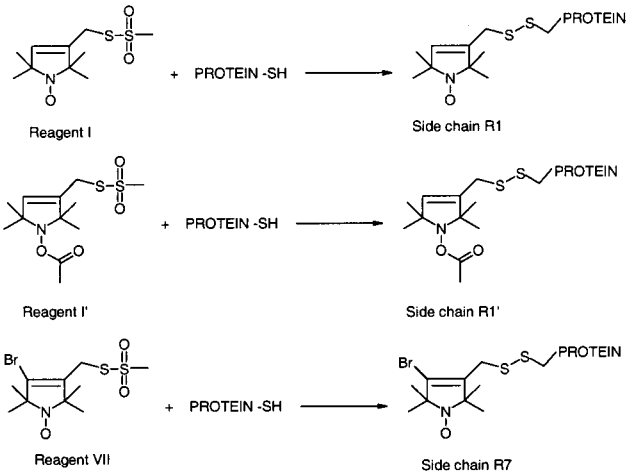

FIGURE 1: Structures of the spin-label reagents and the corresponding side chains produced by reaction with cysteine.

Quantitative distance measurements between pairs of nitroxides can be made under two limiting conditions where theoretical treatments are available for analysis of the data. These are the so-called rigid lattice condition, where the spins are immobile, and the rapid tumbling limit, where the interspin vector tumbles sufficiently rapidly in the laboratory

† Research reported here was supported by NIH Grant EY05216 (W.L.H.), the Jules Stein Professorship (W.L.H.), grants from the Bruce Ford Bundy and Anne Smith Bundy Foundation (W.L.H.), the Hungarian National Research Foundation (Grant OTKA T030013) (K.H.), and the Hungarian Ministry of Education (Grant FKFP 0252/1999) (K.H.).

* To whom correspondence should be addressed: Jules Stein Eye Institute, UCLA School of Medicine, Los Angeles, CA 90095-7008. Telephone: (310) 206-8830. Fax: (310) 794-2144. E-mail: hubbellw@jsei.ucla.edu.

‡ University of California.

§ Current address: Dana-Farber Cancer Institute, 44 Birney, Boston, MA 02115.

|| University of Pécs.

[1] Abbreviations: DTT, dithiothreitol; EDTA, ethylenediaminetetraacetic acid; EPR, electron paramagnetic resonance; SDSL, site-directed spin labeling; T4L, T4 lysozyme.

10.1021/bi011544w CCC: $20.00
Published on Web 11/29/2001

frame to average the dipolar interaction and to induce T_2 relaxation effects.

For the rigid lattice case, there is a large amount of literature beginning with the early work of Likhtenstein and co-workers (reviewed in ref *16*). Current work in the field has been recently reviewed (*17*, *18*). A notable advance that promises to extend the range of the measured distance is the double-quantum coherence method introduced by Freed and co-workers (*19*). Of particular relevance to the results presented here are studies of spin−spin interactions in spin labeled insulin crystals (*20*) and synthetic helical peptides in frozen solutions (*21*). In these studies, it was assumed that (1) the orientation of the interspin vector between the nitroxide groups was randomly distributed in the laboratory reference frame and (2) the orientation of one nitroxide ring relative to the other was randomly distributed. This latter assumption is supported by the disorder of the nitroxide ring in T4L at solvent-exposed sites in high-resolution crystal structures (*22*). In situations where these assumptions are valid, the EPR spectrum can be treated as a convolution of the sum of the spectra of R1 at the individual sites with an appropriate broadening function to represent the dipolar interaction. Alternatively, the spectrum of interacting pairs can be deconvoluted with the sum of the individual spectra to yield the apparent broadening function, from which the interspin distance can be determined (*21*).

If the two nitroxides have a fixed relative orientation, the orientation dependence of the dipolar interaction strength is directly coupled to the spectral anisotropy and the dipolar broadening will thus be a function of magnetic field. Because convolution methods assume a uniform broadening function across the entire spectrum, they cannot be used in such a situation. Hustedt et al. (*23*) have shown that it is possible to simultaneously obtain distance and orientation in such a system by using detailed simulations of spectra taken at different microwave frequencies.

The disadvantage of the rigid lattice analysis is that it requires either a solid at ambient temperature or a frozen solution. Because most protein systems of interest are not in the solid state, frozen solutions are the rule for application of rigid lattice theory. This makes it impossible for real-time detection of distance changes during function.

At the other extreme, the rapid tumbling limit, Redfield relaxation theory has been used to derive interspin distances in spin labeled T4L (*24*). The advantage of this approach is that it can be employed at room temperature, but the disadvantage is that it is limited to proteins with an isotropic correlation time of a few nanoseconds or shorter.

Although interspin distances can be estimated in the rigid lattice and fast tumbling limits by existing methods, neither of these limiting conditions is generally fulfilled at physiological temperatures. A common example is a high-molecular weight soluble or membrane-bound protein where the rotational correlation time (τ_R) is slow on the EPR time scale. For a pair of spins rigidly attached to such a protein, the correlation time of the interspin vector (τ_v) is equal to τ_R. As long as $\tau_R \geq (r^3h)/(3\pi g^2\beta^2)$, the motion of the interspin vector is sufficiently slow not to average the major dipolar anisotropy, that is, to be approximately in the rigid lattice condition (r is the interspin distance, h is Planck's constant, g is the g factor, and β is the Bohr magneton). However, each individual nitroxide generally has motion relative to the protein at physiological temperature, and the rigid lattice condition does not rigorously apply. There is no published theory to account for the dipolar interaction together with the dynamical effects of the spin motion on the EPR spectrum, and the magnitude of dynamical effects on the estimated distance is unknown.

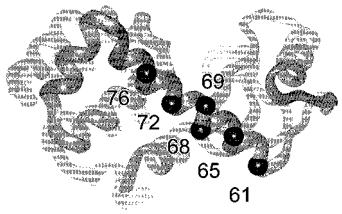

FIGURE 2: Ribbon model of T4 lysozyme showing the location of sites used in the various spin pairs that were investigated. The spheres mark the α-carbon atom of the residues, which are located at every turn of the helix from position 61 to 76.

The purpose of this study is to empirically evaluate the use of rigid lattice theory to estimate distances at physiological temperatures where the correlation time of the interspin vector meets the above condition, and where the individual nitroxide side chains have rapid internal motions (nanosecond correlation time) relative to the protein. Two different nitroxide side chains are evaluated, the commonly employed R1 and the 4-Br derivative designated R7 (Figure 1). In the pyrroline series of nitroxides, position 4 substituents, such as the Br of R7, restrict the amplitude of internal bond rotations in the side chain, leading to a higher degree of order compared to that of R1 (*25*, *26*). Thus, R7 should more closely approach rigid lattice conditions at physiological temperatures, although some orientation effects may be introduced.

T4 lysozyme was chosen as a host for introduction of the spin labels. Pairs of nitroxide side chains were placed along the interdomain helix at solvent-exposed sites with the second residue spaced at $i + 4$ (pairs of residues 61 + 65, 65 + 69), $i + 7$ (pairs of residues 61 and 68, and 65 and 72), $i + 11$ (pair of residues 65 and 76), and $i + 15$ (pair of residues 61 and 76) (Figure 2). EPR spectra of the double mutants were recorded in a 40% sucrose solution, where the correlation time of T4L (∼30 ns) is just long enough to prevent averaging of the main dipolar anisotropy even for the longer distances measured (∼20 Å).

Because the sites of introduction of the nitroxide side chain are all solvent-exposed, little perturbation of the protein structure is expected. This expectation is supported by the relatively small effect of the R1 mutation on both enzymatic activity and thermal stability of the protein at such sites (*25*). In addition, the crystal structures of T4L bearing the R1 residue at solvent-exposed helical sites are virtually identical with the wild-type structure (*22*).

The strategy employed in these experiments is to use rigid lattice conditions (frozen solutions) to estimate interspin distances and distance distributions using a deconvolution method. The results are used as references, and are compared to those obtained using the same analysis applied to ambient temperature data, as a function of viscosity, for both R7 and R1. The results indicate that, within the uncertainty of the determination, the effect of internal motions in the nitroxide side chains on the estimated distance is small, although the spectra of R7 are somewhat better fit by rigid lattice theory.

Thus, it is concluded that rigid lattice theory may be used to estimate interspin distances and distributions at physiological temperatures.

The distance distributions suggested by this analysis are in accord with rotamers of the R1 side chain on helix surface sites in T4L deduced from crystal structures (*22*). In general, the rather broad distributions place practical limitations on the interpretation of interspin distances between R1 residues in terms of protein structure, i.e., in terms of the corresponding inter-Cα distance. It is concluded that structure mapping should involve multiple distance determinations, and that recognizable patterns in distance geometry are the most reliable means for deducing features of a protein fold. In principle, a suitable rotamer library for the R1 side chain can be used in data refinement to improve the accuracy of estimation of inter-Cα distances.

EXPERIMENTAL PROCEDURES

Preparation of Mutants, Spin Labeling, and EPR Spectroscopy. The cysteine-less pseudo-wild-type T4L gene containing the substitutions C54T and C97A (*27*) was kindly provided by F. W. Dahlquist (University of Oregon, Eugene, OR). All the single- or double-cysteine substitutions were introduced into the pseudo-wild-type T4L gene by the overlap extension method (*28*), as previously described (*25*). The nucleotide sequence was verified by sequencing the entire gene.

All mutants of T4L were expressed in *Escherichia coli* K38 cells as previously described (*29*) with some modifications. Briefly, K38 cells containing mutant plasmids were cultured overnight in LB medium containing 100 μg/mL ampicillin. LB medium (0.5 L) containing 100 μg/mL ampicillin was inoculated with 15 mL of the overnight culture. The cells were grown at 37 °C until the optical density at 580 nm reached ~1.0−1.2. Protein expression was induced by adding isopropyl D-thiogalactoside (1 mM). After 1 h, the cells were harvested by centrifugation, and the cell pellets were stored at 20 °C. For protein purification, cell pellets were thawed and resuspended in a buffer containing 20 mM Tris, 1 mM EDTA, 0.02% (w/v) NaN_3, and 10 mM DTT (pH 7.6). The bacterial cell walls were disrupted by sonication on ice, and the cell debris was removed by centrifugation. The supernatant was then loaded onto a Pharmacia Resource S column equilibrated with the buffer containing 0.5 mM DTT. The protein was eluted with a linear gradient of 0 to 1 M NaCl. The T4L fraction was collected; DTT was added to a final concentration of 5−10 mM, and the sample was frozen for storage at −80 °C.

For spin labeling, DTT was removed by gel filtration on a Superdex 75 column (Amersham-Pharmacia), eluting with a buffer containing 20 mM Tris, 150 mM NaCl, and 1 mM EDTA (pH 7.6). The T4L mutants were immediately reacted with an approximately 20-fold excess of either reagent I, reagent VII, or a mixture of I and I= (1:3 molar ratio) at room temperature (Figure 1). The reaction was allowed to continue overnight, and excess reagent was then removed by gel filtration on the Superdex 75 column (Amersham-Pharmacia), eluting with the same buffer used for spin labeling. Labeled proteins were concentrated using a centrifugal concentrator with a cutoff of 10 kDa (Microsep, Filtron Technology Corp., Northborough, MA). The labeling reagents I (*30*, *31*), I= (*7*), and VII (*32*) were synthesized as reported.

EPR spectra were recorded on a Varian 109 spectrometer fitted with a loop gap resonator (*33*). Samples were contained in quartz capillaries at room temperature (22 ± 2 °C) or −180 °C for spectra in frozen solutions. The incident microwave power level was 2 mW for room-temperature samples and 200 μW for frozen solutions.

Determination of Distance Distributions from the Interacting and Noninteracting Line Shapes by an Interactive Convolution−Deconvolution Procedure. (1) Convolution−Deconvolution Procedures. It is assumed that the EPR spectrum of a mutant containing an interacting nitroxide pair (*D*) can be represented as the convolution of the spectrum in the absence of the interaction (*S*) with a broadening function (*B*) that depends on the interspin distance *r* (*21*). Thus, $D = F^{-1}\{F(S) \times F(B)\}$, where *F* and F^{-1} are the forward and inverse Fourier transform operators, respectively. As in previous work (*21*), the broadening function is taken to be the Pake function (*35*) for randomly oriented spin pairs at a fixed distance *r*, and in the absence of motion. For a distribution of interspin distances, the broadening function is then a weighted sum of Pake functions corresponding to the distances that are represented. Similarly, *B* can be experimentally determined by deconvolution of *D* with *S*. Thus, $B = F^{-1}\{F(D)/F(S)\}$. Because deconvolution of a pair of first-derivative spectra yields the same broadening function as the deconvolution of the corresponding absorption spectra, it is convenient to do these operations directly on the first-derivative spectra obtained experimentally. The deconvolution makes no assumptions about the type of interaction. However, if *B* can be represented as a weighted sum of Pake functions, it is possible to interpret the dipolar interaction in terms of an underlying distance distribution using the known distance dependence of the Pake function (*35*). Deconvolution is an inherently unstable algorithm because it involves division of two Fourier transforms. For example, if a spectrum is relatively noise-free, most of the higher-frequency components are near zero. If the Fourier transform of this spectrum is in the denominator, the division results in large high-frequency components that will obscure the form of the deconvoluted line shape *B*. It has been found that adding a slight bias (<0.01%) to all AC components of the transform of *S* can, in most cases, provide a nearly noise-free broadening function *B*. Alternatively, simple low-pass filtering can also be used.

(2) Spectra for the Noninteracting Spin Pairs. The deconvolution analysis requires the spectrum of each double mutant in the absence of dipolar interaction (*S*). Two approaches were used to obtain the noninteracting reference spectra. In the first, EPR spectra were recorded for two T4 mutants, each containing a single nitroxide corresponding to one of the sites in the double mutant. These, as for all raw EPR spectra, were interactively processed to remove simple baseline artifacts (slope, offset) and phase error and were normalized for unit area and 200 G scan range (for data recorded under other scan widths). The underlying line shape of the double mutant in the absence of dipolar interaction was assumed to be the average of the two respective single spectra.

Alternatively, the noninteracting spectra were obtained by reacting the double mutant with a mixture containing a 1:3

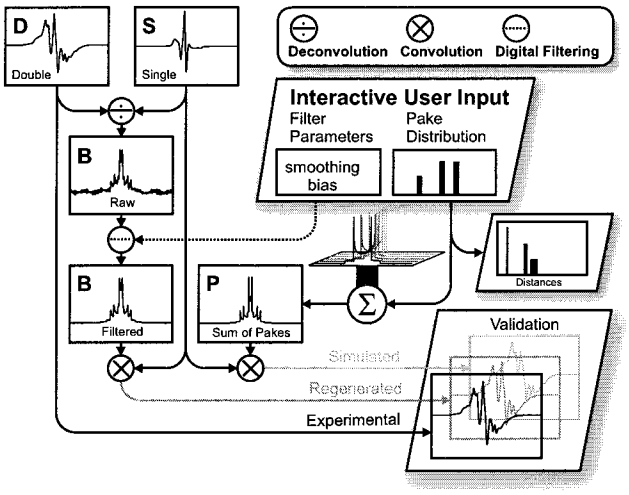

FIGURE 3: Flowchart of the interactive fitting procedure (see the text for details). Symbols representing various mathematical operations are defined in the upper right corner. The spectrum of the double mutant (*D*), and the corresponding noninteracting line shape (sum of singles, *S*), are shown in the top left corner. The *S* and *D* spectra are deconvoluted and filtered to obtain the broadening function (*B*). A user-selectable algebraic sum of theoretical Pake functions (*P*) is constructed to simulate *B*. At the same time, this provides a corresponding distribution of distances. For validation, regenerated and simulated spectra are compared with the original experimental double spectrum (bottom right corner). The regenerated spectrum, the convolution *SB*, is a measure of artifacts introduced by filtering of *B*. The simulated spectrum, the convolution *SP*, shows how well *P* represents the broadening function.

molar ratio of spin-label (I) and the diamagnetic analogue (I′) (Figure 1). If equal reactivity and 100% labeling are assumed, this will give a statistical distribution of product where $^{15}/_{16}$ of the protein molecules will have one or fewer R1 distributed randomly between the two sites. Thus, the spectrum is predominantly that of the noninteracting line shape (the sum of the spectra of the individual sites, without the effect of the magnetic interaction). The remaining $^{1}/_{16}$ interacting component that contains two R1 side chains can be cleanly subtracted using the spectrum obtained from the protein labeled with pure reagent (I).

(3) Fitting and Determination of Distance Distributions. The interactive fitting to find a set of Pake functions representing the experimental *B* function determined by deconvolution was done using a program written in LabVIEW (National Instruments). Any parameter or input change triggers a full recalculation and display of all results. This takes only fractions of a second, and the overall impact can be immediately observed. A simplified flowchart of the program is shown in Figure 3. As a first step, the program reads the first-derivative spectra *S* and *D*, deconvolutes *D* with *S*, and displays *B*. The following parameters are then adjusted for optimization of *B*: (1) bias of the Fourier transform of *S* (see above) and low-pass filtering the deconvolution *B* and (2) horizontal shift of *D* to center the deconvolution in case *S* and *D* were not perfectly aligned. Once the deconvolution is centered, it can optionally be averaged with its mirror image to force symmetry and improve the signal-to-noise ratio. (3) In rare cases, it was also necessary to remove spurious baseline oscillations with selectable narrowband filters. As a consistency check, the filtered and processed broadening function is convoluted with *S* to regenerate a first-derivative spectrum *R*. If *R* and *D* were similar, the filtering and symmetry operations did not introduce excessive artifacts.

Following these initial operations, program inputs allow the generation of a function *P* consisting of a normalized sum of up to 50 weighted Pake functions, representing different interspin distances. At the same time, a properly weighted histogram is generated to display the corresponding distance distribution. The composition of *P* is modified to obtain a fit of *P* to *B*. Simultaneously, *P* is also convoluted with *S* to generate *PS*, which represents a simulation of the interacting spectrum *D*. Minor adjustments to *P* are now used to further improve the fit between *D* and *PS*. The presence of a noninteracting component, for example, caused by incomplete labeling, is easily modeled by adjusting the amount of a degenerate zero-width component in *P* (infinite distance). Because all spectra are normalized for the same number of spins, *B* has unit area. Since *P* is also normalized for unit area, *D* and *PS* are also normalized. All spectral amplitudes are internally consistent and not independently adjustable.

RESULTS

EPR Spectra of R1 and R7 Single Mutants. The EPR spectra of R1 at each of the individual sites except for position 68 have been previously published (*24*, *25*, *32*) and are reproduced in Figure 4a for reference, along with that of 68R1. Residues 68R1, 72R1, and 76R1 have spectra reflecting anisotropic motion typical of noninteracting, solvent-exposed, helix surface sites (*25*, *26*). Residue 61R1 is at the N-terminus of the helix, and has two spectral components, presumably reflecting two side chain populations with different mobilities, typical of such sites (*25*). Residues 65R1 and 69R1 may also have multiple dynamic components reflecting some degree of tertiary interaction. The EPR spectra for R7 at each of the sites are shown in Figure 4b. As can be seen, the spectra are much broader, reflecting a higher degree of order (less mobility) for R7 at each site compared to the corresponding R1 derivative.

Dipolar Interactions of R1 in Frozen Solution. Figure 5 shows the experimental data and analysis for each of the double mutants of R1 investigated in the frozen state. Panel a for each mutant shows the spectrum of the double mutant (*D*, dark trace) compared with the algebraic sum of the spectra of the corresponding single mutants (*S*, light trace), each normalized to the same number of spins. The sharply reduced spectral amplitude of *D* for double mutants 61R1+65R1, 65R1+69R1, and 61R1+68R1 relative to that of *S* attests to the strength of the dipolar interaction that broadens the spectrum. The slight reduction in the amplitude of *D* relative to that of *S* for 65R1+76R1 and 61R1+76R1 indicates a weak interaction with slight broadening that would be difficult to detect without a very good signal-to-noise ratio. These represent the limit of detection for nitroxide−nitroxide dipolar interactions by the methods described here.

Panel b shows the broadening function *B* obtained by deconvolution of *D* with *S* (light trace). For the strongly interacting pair (61R1+65R1), the result has the form of a sum of Pake functions representing a narrow distribution of interspin distances. For 65R1+69R1 and 61R1+68R1, the broadening functions have in addition a relatively sharp central feature. In 65R1+69R1, this feature is sufficiently

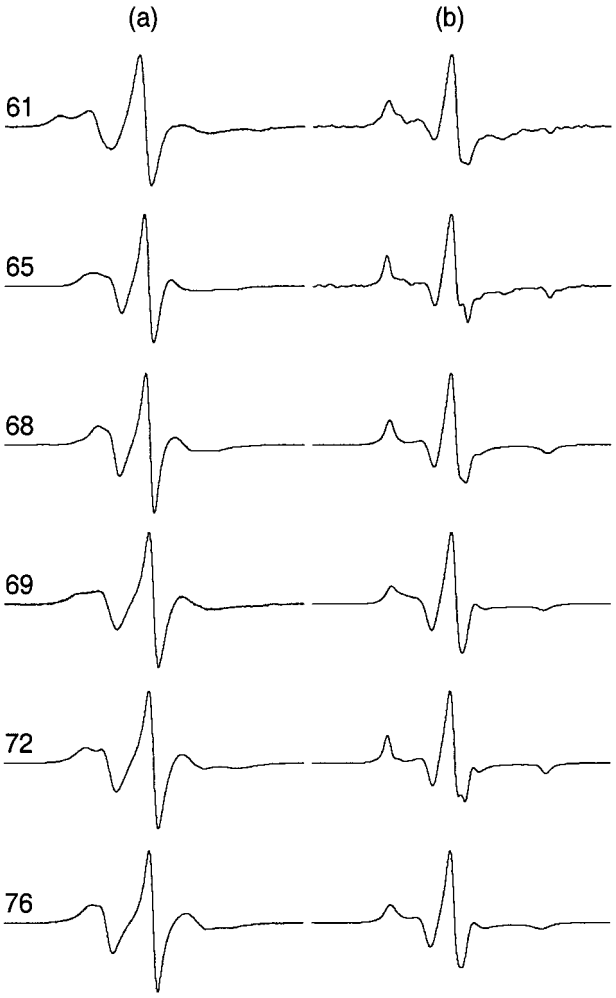

FIGURE 4: EPR spectra for the spin-labeled side chains at the indicated sites in T4L in a 40% sucrose solution at room temperature: (a) R1 and (b) R7. The scan width is 100 G.

broad to represent a population of spins with a large interspin distance and an unresolved splitting. This population is recognizable in the EPR spectrum of the double mutant as the sharp components superposed on a broader background (panel c, dark trace). In 61R1+68R1, the central feature is narrow, and likely represents a small percentage of singly labeled protein with noninteracting spins (*21*), although one cannot exclude the possibility of a small population of spins at a large distance. For 65R1+76R1 and 61R1+76R1, *B* is a relatively narrow line with no resolved structure, as expected for a large (>20 Å) interspin distance. For both of these double mutants, the breadth of the $m_I = 0$ resonance line is measurably larger than that for the sum of the single mutants and the deconvolution shows a broadened peak. Thus, although the effects are small, it is likely that the width of the broadening function does in fact arise from a weak dipolar interaction. However, distances determined from this function are intrinsically less reliable than those from more strongly interacting pairs (see below). The dark trace in panel b is a sum of Pake functions (*P*), representing a distribution of distances that simultaneously provides a fit to *B* and a fit of the simulated EPR spectrum to that of the double mutant.

Panel c compares the experimental spectra for the double mutant *D* (dark trace) and the spectrum simulated by convolution of *P* with *S* (light trace). In each case, the simulated and experimental spectra are in reasonable agreement. For 61R1+65R1, the general features are well fit and some, but not all, of the detailed features are reproduced. This double represents the most difficult situation for simulation, that is, a closely spaced pair of spins where the assumption of random relative orientations is critically tested. Rather small net orientations could account for the imperfections in the fit, and very slight changes in distance and/or distance distribution cause drastic changes in the simulated spectrum that seriously degrade the quality of the fit.

Finally, panel d is the distribution of distances corresponding to the simulated Pake function of panel b. The bimodal distribution for 65R1+69R1 may represent two rotameric states of either 65R1 or 69R1 in the frozen state. The distribution for 61R1+68R1 may also be bimodal.

Dipolar Interactions at Ambient Temperature. (1) Effect of Viscosity. At physiological temperatures, T4L undergoes rotary motion that results in partial or complete averaging of dipolar interactions (*24*). The correlation time needed to average the interaction depends on the strength of the interaction, and hence on the interspin distance. For each pair of interacting spins that was investigated, the spectra were recorded as a function of solution viscosity by changing the concentration of sucrose in the range of 0−55% (w/w). At 22 °C, this corresponds to an increase in viscosity from approximately 1 to 40 cP, and a corresponding increase in τ_R of T4L from approximately 6 to 240 ns, assuming Stokes−Einstein behavior. For the individual single mutants labeled with either R1 or R7, the spectra were relatively unchanged by increasing sucrose concentrations from ∼30 to 55% (data not shown), indicating that the sucrose in that range did not directly alter the dynamics or conformation of the nitroxide side chain.

As an example of the effect of the correlation time on the dipolar interaction, Figure 6 illustrates the effect of sucrose concentration on the EPR spectra, on the deconvolutions, and on the simulated spectra and distance distributions for the double mutant 65R7+69R7. The organization of panels in Figure 6 is the same as that for Figure 5. As the sucrose concentration is increased from 0 to 40%, corresponding to a viscosity change from ∼1 to 5.7 cP, the overall spectral breadth of the double mutant changes little (panel c, dark trace).

As shown in panel b, the deconvolution function *B* obtained at 22 °C has the shape of a broadened Pake function, like that in frozen solution, at all sucrose concentrations. Both *B* and the distance distribution (panel d) are relatively insensitive to viscosity, although the contribution from a longer distance component, seen in the central region of the *B* function at 40% sucrose (arrow), is not resolved at lower viscosities. In addition, the apparent splitting of the Pake-like *B* function increases slightly with increasing viscosity. That the *B* function is affected relatively little by correlation time is expected for short interspin distances, because the breadth is dominated by the strongest dipolar interaction that is not averaged. The effects of sucrose on the other strongly interacting pairs are similar for both R1 and R7.

As shown in panel c, the simulated spectrum (dark trace) is a rather poor fit to the data for the 0% sucrose case (light trace). This can be attributed to the onset of some averaging of the dipolar interaction for the rapid tumbling. The simulated dipolar-coupled spectra are relatively good for 20−

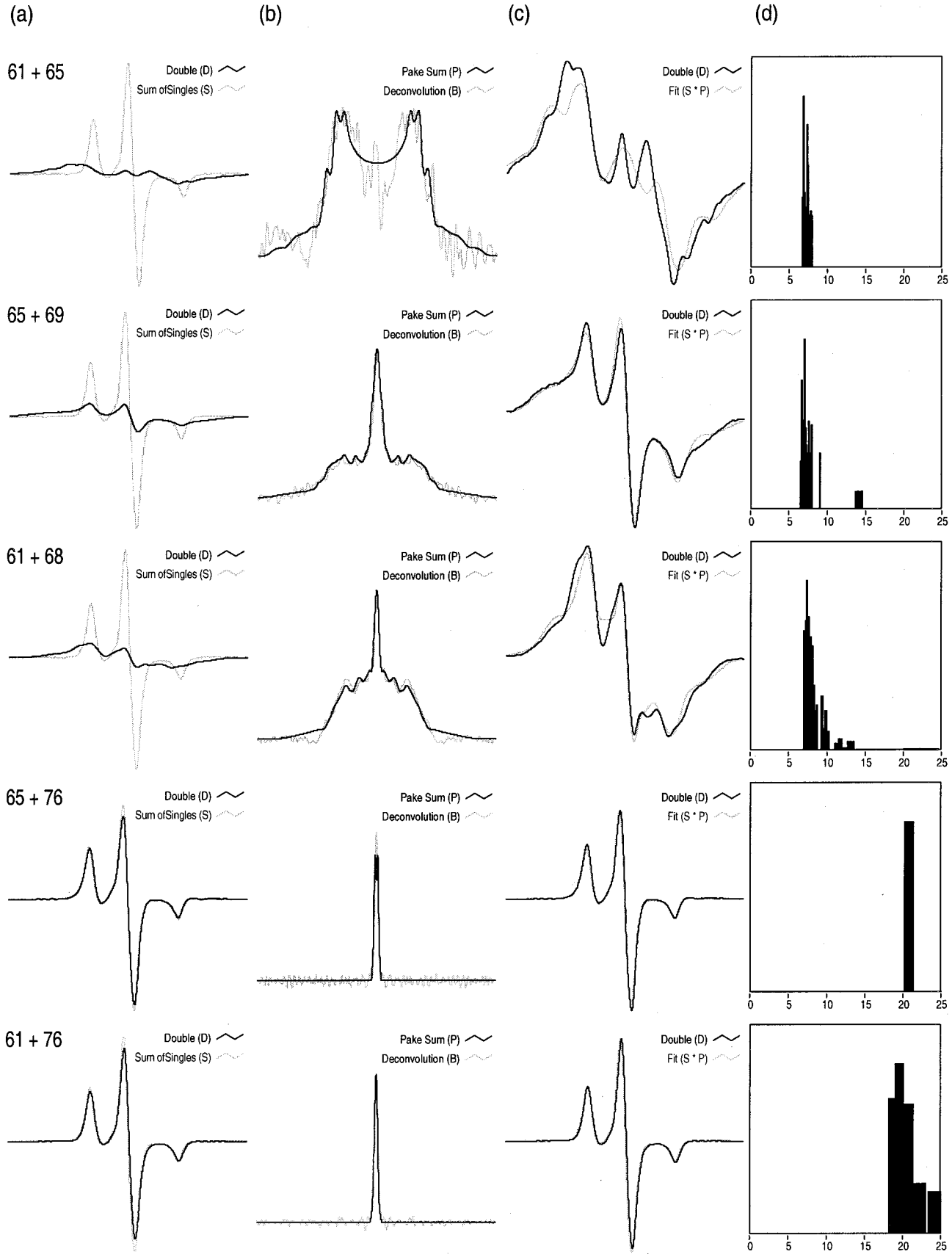

FIGURE 5: Analysis of spectra of interacting R1 spin pairs in T4L in frozen solution. For each spin pair, panel a compares the experimental spectrum of the double mutant (*D*, dark trace) with the sum of the spectra of the corresponding single mutants, normalized to the same number of spins (*S*, light trace). Panel b compares the deconvolution of *D* with *S* (*B*, light trace) and the sum of Pake functions (*P*, dark trace) that represents a fit to *B*. Panel c compares *D* (dark trace) with the simulated spectrum (*S* convoluted with *P*, light trace; see the text). Panel d is the distance distribution corresponding to the sum of Pake functions in angstroms (*P*).

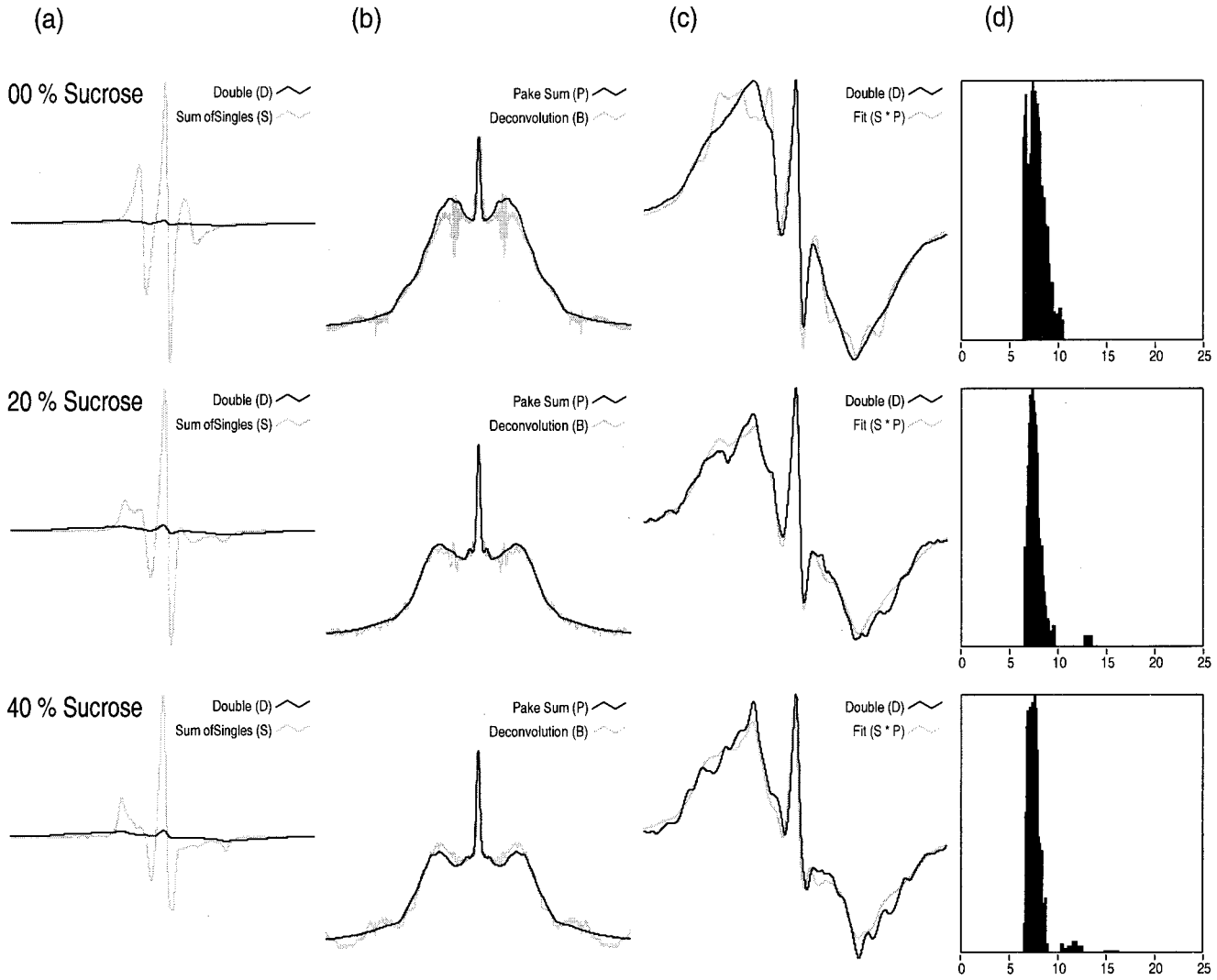

FIGURE 6: Analysis of spectra for 65R7+69R7 in T4L in solution as a function of sucrose concentration at 22 °C. For each sucrose concentration (w/w), panel a compares the experimental spectrum of the double mutant (*D*, dark trace) with the sum of the spectra of the corresponding single mutants, normalized to the same number of spins (*S*, light trace). Panel b compares the deconvolution of *D* with *S* (*B*, light trace) and the sum of Pake functions (*P*) that represents a fit to *B*. Panel c compares *D* (dark trace) with the simulated spectrum (*S* convoluted with *P*, light trace; see the text). Panel d is the distance distribution corresponding to the sum of Pake functions in angstroms (*P*).

40% sucrose. It is important to note that even the poorer fits at low viscosities provide similar distances.

(2) Dipolar Interactions between R7 Residues. Interactions between R7 residues will be considered first, because the more constrained motion of this side chain at room temperature is most similar to rigid lattice conditions in frozen solution. In this series, an additional pair, 65R7+72R7 (i + 7), has been investigated.

For each interacting pair of R7 residues that was investigated, the spectra obtained at 40% sucrose were analyzed to determine the broadening function, to simulate the spectra of the double mutants, and to obtain the interspin distance distribution. Figure 7, organized in the same way as Figures 5 and 6, gives the results. As expected, the pairs 61R7+65R7, 65R7+69R7, 61R7+68R7, and 65R7+72R7 all show strong to moderate interaction judging by the reduction in the amplitude of the spectrum for the double mutant compared to that for the sum of the single mutants, and the shape of the broadening function. Although the spectra are quite different in detail from those of the R1 doubles in frozen solution, the derived distance distributions are very similar. The distance distributions of 65R7+69R7 and 61R7+68R7 are bimodal, just as for the corresponding R1 derivatives in frozen solution. For 65R7+69R7, the mode of the dominant population at short distance lies at ~7−8 Å, the same as for the corresponding R1 derivative in frozen solutions. The minor population is relatively broad, with the mode at a distance slightly shorter than that of the R1 derivative. For 61R7+68R7, the mode for the population corresponding to the closer distance is at ~7−8 Å, again the same as that for the R1 derivative in frozen solutions. The population at longer distances is more significant for R7, as can be readily appreciated from the distinct contributions to the broadening function, with the mode at slightly longer distances than for the R1 derivative in frozen solutions. The distance distribution for 65R7+72R7 is bimodal, with one mode at ~12 Å and the other at ~16 Å.

(3) Interactions between R1 Residues. As for the R7 residues, interactions between the more mobile R1 residues were investigated in a 40% sucrose solution at 22 °C. The

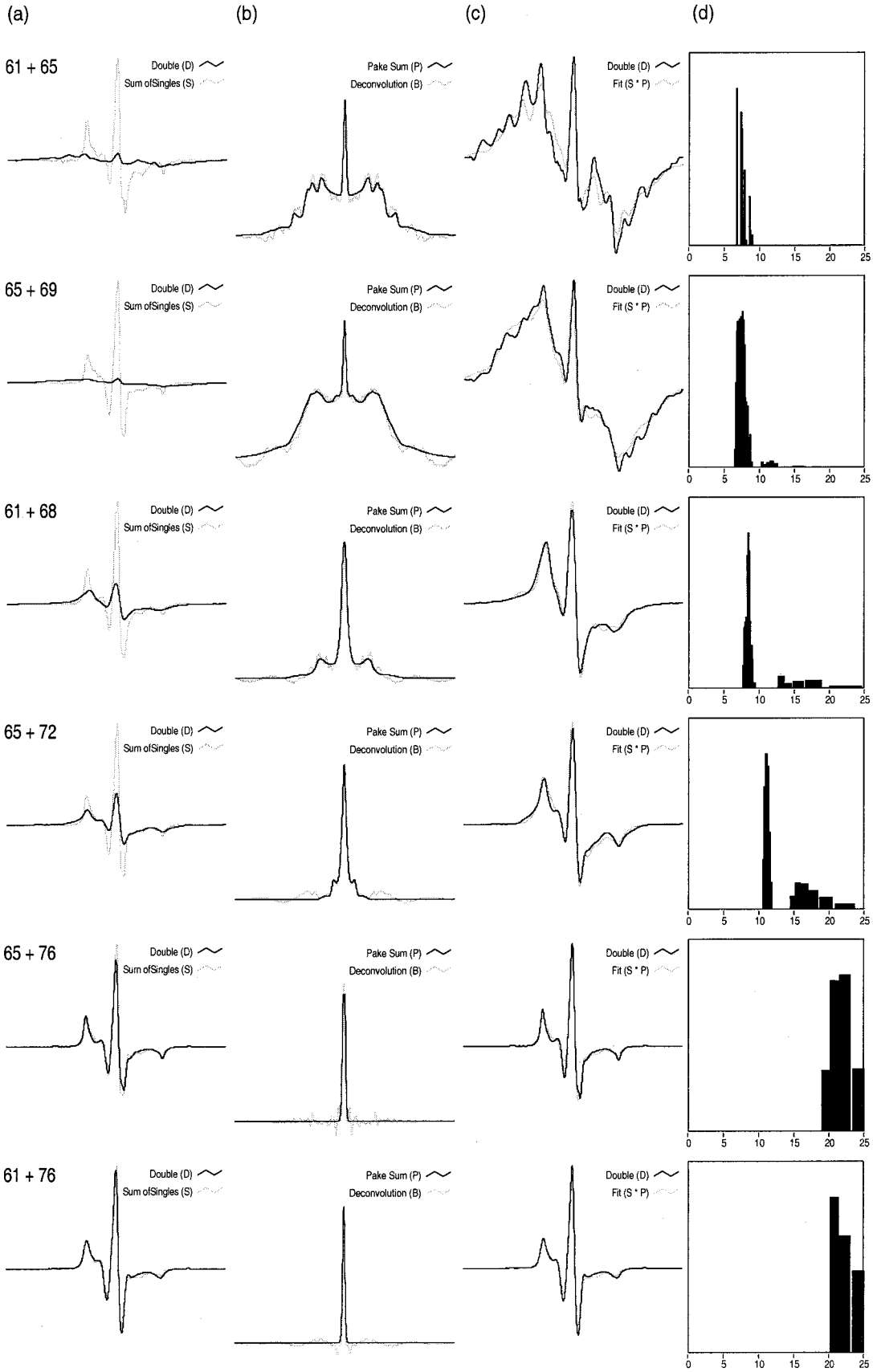

FIGURE 7: Analysis of spectra of R7 spin pairs in T4L in a 40% sucrose solution at ambient temperature. For each spin pair, panel a compares the experimental spectrum of the double mutant (*D*, dark trace) with the sum of the spectra of the corresponding single mutants, normalized to the same number of spins (*S*, light trace). Panel b compares the deconvolution of *D* with *S* (*B*, light trace) and the sum of Pake functions (*P*, dark trace) that represents a fit to *B*. Panel c compares *D* (dark trace) with the simulated spectrum (*S* convoluted with *P*, light trace; see the text). Panel d is the distance distribution corresponding to the sum of Pake functions in angstroms (*P*).

data and results of the analysis are shown in Figure 8, which is again organized in the same fashion as Figures 5−7. The analysis illustrates a new feature, namely, the use of the diamagnetic analogue R1′ to obtain the spectra of the noninteracting spins for the 61R1+65R1 and 65R1+69R1 pairs (see Experimental Procedures). For these cases, the spectrum obtained from labeling the double cysteine mutant with a dilute mixture of R1 in R1′ was virtually identical to the corresponding sum of the single mutants. This suggests that mutual steric interactions between the labels at these closely spaced sites do not drastically alter their dynamic modes.

For the sites that can be compared, the interspin distance distributions for R1 residues in the frozen state (Figure 5) and at room temperature (Figure 8) are very similar. The comparison of distance distributions at room temperature for R7 (Figure 7) and R1 (Figure 8) pairs also reveals an overall good agreement, with 65R1+72R1 showing the only significant difference. For both R1 and R7, the distribution of 65R1+72R1 is bimodal, but both modes are shifted to shorter distances for R1 pairs (by ∼3 Å). The distributions for R1 pairs are also greater in width than for R7 pairs.

Comparison of the Experimentally Determined Distances with Predictions Based on Modeling. As shown above, comparison of the distance distributions from R1 pairs in frozen solution and R1 and R7 pairs at room temperature in 40% sucrose reveals an overall gratifying similarity (Figures 5−8). To compare these results with expectations from the known structures of the protein and side chain, the R1 side chains at the various sites were modeled in conformations where $X_1 = X_2 = 300°$ and $X_3 = 270°$ (designated the $g^+g^+g^+$ rotamer) or $X_1 = 180°$, $X_2 = 60°$, and $X_3 = 90°$ (the tg^-g^- rotamer; see Figure 9a for numbering of the dihedral angles). The g^+g^+ and tg^- states for X_1X_2 were identified in crystal structures of T4L for R1 at helix surface sites, and the conformations for X_3 were inferred from the location of diffuse electron density and steric considerations (*22*). The X_4 and X_5 dihedral angles for helix surface sites could not be determined from the crystal structures because electron density was not well resolved for the mobile nitroxide ring. Of these two angles, X_4 is the primary determinant of the ring position. In both the $g^+g^+g^+$ and tg^-g^- states, a wide range of values of X_4 is allowed, and undoubtedly, distributions in this angle make major contributions to the distribution in distances observed experimentally. Rotation about X_4 moves the nitrogen atom of the nitroxide on a circle of diameter ≈6 Å (Figure 9a). Thus, in the absence of other interactions, the interspin distance between an R1 nitroxide pair could have a distribution width of 12 Å breadth at the extremes, and some of the data show such breadth (Figure 8). Thus, the distribution widths are physically reasonable, but their precise interpretation must remain tentative pending further studies.

For illustrative purposes, Figure 9b shows models of the R1 side chain at each site in the $g^+g^+g^+$ conformation with values of X_4 chosen to simultaneously achieve (1) an energy-minimized conformation with respect to the X_4 and X_5 dihedrals and (2) agreement with distances measured experimentally at 22 °C for R1 pairs. For the bimodal distributions 65R1+69R1, 61R1+68R1, and 65R1+72R1, the side chains are modeled to account for the populations with the closest distances. The populations with the longer distances in the bimodal distributions can be readily accounted for either by a second state of 65R1 or 68R1 in the tg^-g^- conformation or by a suitable choice of X_4 (models not shown). The important point is that such global agreement can be readily achieved with favorable side chain conformations, a fact that can be appreciated by comparison of the experimental distances given in Figures 5−8 with those shown in Figure 9b.

DISCUSSION

Interspin Distances in Frozen Solutions. The deconvolution approach used in the studies described above was previously employed to analyze dipole interactions between R1 side chains on helical peptides in frozen solution (*21*). In that work, the derived broadening functions were relatively featureless, and were taken to be the sum of essentially a continuum of Pake functions resulting from a broad range of internitroxide distances. The broad distance ranges could arise from both disorder in the peptide structure and disorder within the R1 side chain itself. The data presented here extend the work on peptides to include the analysis of R1 interacting pairs on a known and highly ordered α-helical structure in a native protein in frozen solution. In contrast to the peptide data, some of the broadening functions determined by deconvolution have the recognizable shape of a broadened Pake function. Spin pairs involving 61+65, 65+69, and 61+68 are examples (Figures 5−8). Apparently, the interacting pairs are characterized by a distribution of discrete distances, rather than a broad continuum. This is expected for side chains that exist in discrete rotamers (*22*).

For both 61R1+65R1 and 65R1+69R1, the nitroxides are separated by four residues (one turn) along the helix, and the dominant population has an interspin distance of ∼7−9 Å. In 65R1+69R1, the data suggest a second minor population with an interspin distance of ∼14 Å. As mentioned above, this population can be readily accounted for by the existence of a second rotamer of one of the side chains. The room-temperature EPR spectra of 61R1, 65R1, and 69R1 each reveal evidence for multiple dynamic populations of the side chain due to weak interactions. Such interactions provide a rationale for site-dependent rotamer states.

For the double mutant 61R1+68R1, the nitroxides are separated by seven residues (two turns) along the helix. Surprisingly, analysis of the dipolar interaction of 61R1+68R1 in frozen solution indicates that the major population has an interspin distance that is approximately the same as that for R1 residues separated by a single turn. As shown in Figure 9b, this result is readily accommodated with the side chain in the favored $g^+g^+g^+$ conformation by adjustments of X_4 for both 68R1 and 61R1. The value of X_4 for residue 68R1 (∼90°) required to account for the experimentally determined distance can be rationalized by the fact that unfavorable steric interactions of the nitroxide ring occur with Phe 4 for values of X_4 that give larger interspin distances. Nevertheless, there is another significant population with a larger interspin distance centered at ∼13 Å, close to that expected for two turns of a helix.

For the longer distances in 65R1+76R1 and 61R1+76R1 ($r \sim 20-23$ Å), the dipolar interaction is small and difficult to detect under any condition (Figure 5), and the actual value of the distance and the distribution is relatively uncertain.

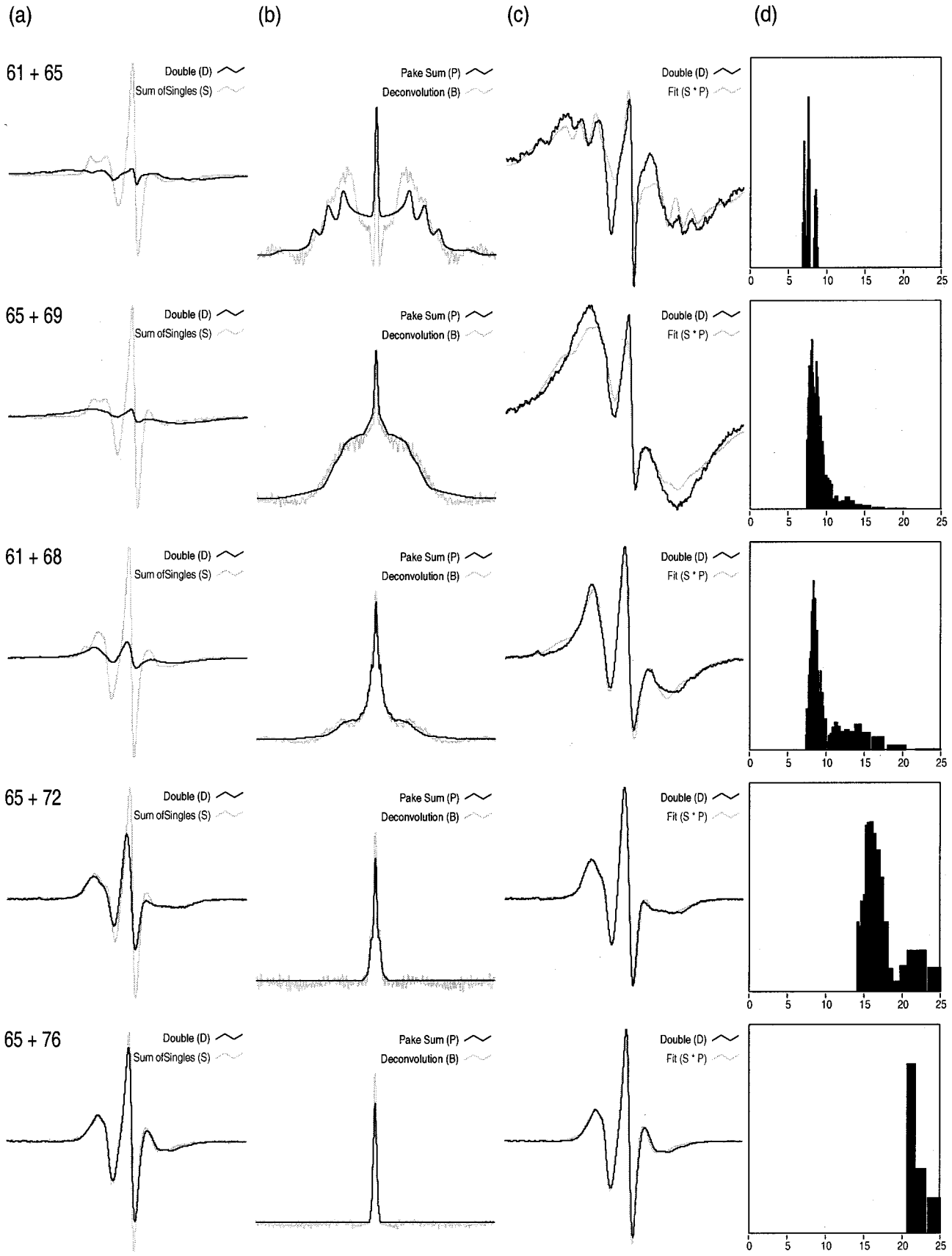

FIGURE 8: Analysis of spectra of R1 spin pairs in T4L in a 40% sucrose solution. For each spin pair, panel a compares the experimental spectrum of the double mutant (*D*, dark trace) with the sum of the spectra of the corresponding single mutants, normalized to the same number of spins (*S*, light trace). Panel b compares the deconvolution of *D* with *S* (*B*, light trace) and the sum of Pake functions (*P*, dark trace) that represents a fit to *B*. Panel c compares *D* (dark trace) with the simulated spectrum (*S* convoluted with *P*, light trace; see the text). Panel d is the distance distribution corresponding to the sum of Pake functions in angstroms (*P*).

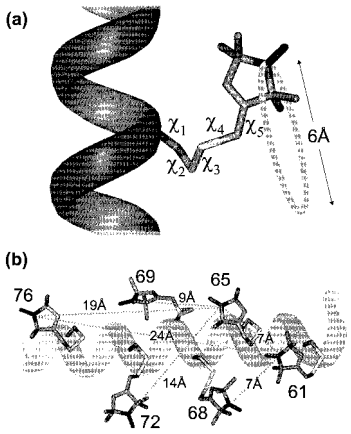

FIGURE 9: Models of the R1 side chain and the expected distances between the various spin pairs. (a) The favored $g^+g^+g^+$ rotamer of the R1 side chain (*22*), identifying the dihedral angles. The cone indicates the locus of points swept out by the nitroxide nitrogen due to rotation about X_4. (b) The R1 side chain at each of the sites investigated, modeled in the $g^+g^+g^+$ rotamer where $X_1 = 300°$, $X_2 = 300°$, and $X_3 = 270°$. Values of X_4 were selected as discussed in the text. The distances shown are those between the nitrogen atoms of the indicated nitroxides.

Within a distribution of distances, the longer distances dominate the spectral intensity and essentially reduce the effective range of distances where quantitative analysis is possible. In such circumstances, a distance of 15−18 Å is probably the practical limit for analysis. However, this is an ideal distance range for mapping helix packing in helical bundle proteins, because the maximum nitroxide R1 separation in adjacent helices is on that order.

The conclusion from the studies in frozen solution is that the assumption of random relative orientations of the nitroxides gives an adequate representation of the system, at least for solvent-exposed helical surface sites. This is concluded from the reasonably good fits of the simulated spectra to the experimental data (Figures 5−8) and the general agreement of the experimental distances with those from modeling. Because rigid lattice theory is applicable to the frozen solution state, the distances resulting from this analysis will be taken as reference values for judging the validity of distance measurement at room temperature, with mobile spins, using rigid lattice theory.

Interspin Distances at Room Temperature. The quantitative estimation of interspin distances from dipolar interactions of nitroxides at physiological temperatures is an important capability for exploring real-time conformational changes associated with function in proteins, and for eliminating possible conformational changes induced by freezing. The data presented above in Figures 5−8 indicate that rigid lattice analysis is suitable for determining interspin distances in the presence of motions of the nitroxides when the correlation time of the interspin vector, τ_v, is such that $\tau_R \geq (r^3h)/(3\pi g^2\beta^2)$. This condition guarantees that the largest dipolar anisotropy is not averaged. For nitroxides linked to rigid protein structures, as is the case here, $\tau_V = \tau_R$, where τ_R is the rotational correlation time of the protein. For spins separated in the 7−10 Å range, $\tau_R > 1$ ns, easily met for T4L in 40% sucrose where $\tau_R \approx 30$ ns. For T4L in buffer alone, $\tau_R \approx 6$ ns. Under this condition, some dipolar interaction is already averaged for 61R7+65R7, as shown in Figure 6. For the longer distances of ∼20 Å, the condition for nonaveraging of the dipolar interaction is a τ_R of >20 ns, and 40% sucrose is just sufficient.

For distances of ∼15 Å or greater, the dipolar interaction is completely averaged for T4L in buffer alone at 22 °C. In this regime, modulation of the dipolar interaction by molecular tumbling induces T_2 relaxation, and Redfield relaxation theory has been employed to estimate nitroxide interspin distances (*24*). In this case, the deconvolution of the spectrum of the double mutant with that of the sum of the singles yields a Lorentzian broadening function as opposed to the Pake-like functions observed here. For ≥50 kDa proteins, distances of up to 20 Å can be determined from dipolar interactions without the use of viscosity-modifying agents. For membrane-bound proteins, the correlation times are very long due to the high effective viscosity of the bilayer, and the direct application of the above analysis should present no difficulty.

The data of Figures 5−8 show that narrow and discrete distributions are obtained for R1 pairs in frozen solution, but that broader, overlapping distributions are the case for R1 at room temperature. The broader distributions may result from a wider distribution of the X_4 dihedral angle at room temperature, or from dynamic effects not considered in this analysis. It is interesting that for 61R1+68R1 at room temperature, a distribution centered at ∼14 Å is well-populated, corresponding to the expected interspin distance for a pair spaced by two helical turns. In frozen solution, this state is minor. Apparently, freezing perturbs the relative rotamer populations.

For analysis of the R1 spin pairs at room temperature, dilute mixtures of R1 in R1′, the diamagnetic analogue of R1, were employed at some sites. As outlined in Experimental Procedures, such a mixture provides directly the spectrum corresponding to the noninteracting spin pair needed for deconvolution and convolution. The advantages of this procedure are twofold. First, it is unnecessary to prepare the individual single cysteine mutants to obtain the corresponding noninteracting spectra. Second, steric interaction between two labels at closely spaced sites may invalidate the use of the sum of the single spectra to represent the noninteracting state. In this case, the use of the R1/R1= mixture is essential.

The position 4 substituent on the nitroxide ring of the R7 side chain strongly restricts rotations about the X_5 dihedral (*26*). Although modulation of this dihedral angle does not significantly change the interspin distance (Figure 9a), it does result in averaging of the major nitroxide magnetic anisotropies. As a result, the R7 side chain has EPR spectra reflecting a higher degree of order relative to R1 (compare panels a and b of Figure 4). The fact that the distance distributions obtained for R1 and R7 at room temperature are very similar thus suggests that the internal bond rotations of the side chain that modulate magnetic anisotropies have little effect on the magnetic dipolar interaction. However, there is an apparent shift in interspin distances between 65R1+72R1 and 65R7+72R7 at ambient temperature, although both show a similar bimodal distribution. This difference could arise from interactions of the 4-Br substituent in R7 with the environment that stabilizes a particular X_4 rotamer.

Implications for Structure Mapping. The results of this study reveal a distribution of interspin distances as anticipated

from the existence of multiple rotamers of the R1 side chain at helix surface sites (*22*). In general, such distributions make it problematic to infer accurate distances between α-carbons of the backbone from distance measurements between nitroxide groups without precise knowledge of the R1 conformations. Any molecular labeling technique that employs probes with internal flexibility faces this problem. In the absence of such information, interspin distance measurements may be still be used to map features of protein tertiary folds, but it is essential to determine distances between multiple pairs and to rely on patterns of distances to deduce structural information, as previously emphasized (*24*). With this strategy, a biased distance due to an unusual side chain conformation can be identified and possible false negatives due to incomplete labeling ignored.

If the site of labeling is on a solvent-exposed surface of a known secondary structure, and R1 makes only weak local interactions, the problem is less severe because the secondary structure-dependent preferred rotamers of R1 can be determined from crystallographic studies (*22*). To employ this kind of information in data refinement will require additional crystal structures of R1 on both α-helical and β structures to provide the required rotamer library.

The interpretation of *changes* in interspin distance in terms of conformational changes may also be subject to errors due to side chain flexibility. In this case, repacking of the side chain between different rotamers could result in interspin distance changes, although the protein backbone may move much less. Buried residues may also have a net orientation with respect to the interspin vector, and a change in orientation alone could give rise to changes in dipolar-coupled EPR spectra. Fortunately, buried sites are readily recognized in the EPR spectra and the results can be evaluated in this context.

One of the most fruitful applications of SDSL distance measurements will be to examine the solution structure and conformational changes of proteins of known crystallographic structure. In such cases, the secondary structure and key features of the local environment of the nitroxide side chain are known. Thus, it is in principle possible to select sites where the preferred rotamer state of the side chain is known from a suitable library. With such information, nitroxide−nitroxide distance mapping may prove to be a relatively high-resolution method for comparison of crystal and solution structures. Many functionally related conformational changes involve rigid-body motions of regular secondary structure (*4*). To quantitatively map such changes in solution, the crystal structure can be used to select sites within sequences of interest that are located on exposed surfaces with no tertiary interactions. Distance changes determined in this way are expected to accurately reflect the relative rigid-body displacement of the secondary structure elements because the environment of the nitroxide side chain is conserved in the motion.

REFERENCES

1. Hubbell, W. L., and Altenbach, C. (1994) *Curr. Opin. Struct. Biol. 4*, 566−573.
2. Hubbell, W. L., Mchaourab, H. S., Altenbach, C., and Lietzow, M. (1996) *Structure 4*, 779−782.
3. Hubbell, W. L., Gross, A., Langen, R., and Lietzow, M. (1998) *Curr. Opin. Struct. Biol. 8*, 649−656.
4. Hubbell, W. L., Cafiso, D. S., and Altenbach, C. (2000) *Nat. Struct. Biol. 7*, 735−739.
5. Feix, J. B., and Klug, C. S. (1998) in *Biological Magnetic Resonance. Volume 14: Spin Labeling: The Next Millenium* (Berliner, L. J., Ed.) pp 252−281, Plenum Press, New York.
6. Perozo, E., Cortes, D. M., and Cuello, L. G. (1998) *Nat. Struct. Biol. 5*, 459−469.
7. Gross, A., Columbus, L., Hideg, K., Altenbach, C., and Hubbell, W. L. (1999) *Biochemistry 38*, 10324−10335.
8. Koteiche, H. A., and Mchaourab, H. S. (1999) *J. Mol. Biol. 294*, 561−577.
9. Poirier, M. A., Xiao, W., Macosko, J. C., Chan, C., Shin, Y. K., and Bennett, M. K. (1998) *Nat. Struct. Biol. 5*, 765−769.
10. He, M., Voss, J., Hubbell, W., and Kaback, H. (1995) *Biochemistry 34*, 15661−15666.
11. Anthony-Cahill, S. J., Benfield, P A., Fairman, R., Wasserman, Z. R., Brenner, S. L., Stafford, W. F., Altenbach, C., Hubbell, W. L., and De Grado, W. F. (1992) *Science 255*, 979−983.
12. Farrens, D. L., Altenbach, C., Yang, K., Hubbell, W. L., and Khorana, H. G. (1996) *Science 274*, 768−770.
13. Xiao, W., Brown, L. S., Needleman, R., Lanyi, J. K., and Shin, Y. K. (2000) *J. Mol. Biol. 304*, 715−721.
14. Tiebel, B., Radzwill, N., Mar, Aung-Hilbrich, L. M., Helbi, V., Steinhoff, H. J., and Hillen, W. (1999) *J. Mol. Biol. 290*, 229−240.
15. Perozo, E., Cortes, D. M., and Cuello, L. G. (1999) *Science 285*, 73−78.
16. Likhtenstein, G. I. (1976) *Spin Labeling Methods in Molecular Biology*, Chapter 3, John Wiley and Sons, New York.
17. Hustedt, E. J., and Beth, A. H. (1999) *Annu. Rev. Biophys. Biomol. Struct. 28*, 129−153.
18. Eaton, G. R., Eaton, S. S., and Berliner, L. J. (2000) *Distance Measurements in Biological Systems by EPR, Volume 19 of Biological Magnetic Resonance*, Kluwer, New York.
19. Borbat, P. P., Costa-Filho, A. J., Earle, K. A., Moscicki, J. K., and Freed, J. H. (2001) *Science 291*, 266−269.
20. Steinhoff, H. J., Radzwill, N., Thevis, W., Lenz, V., Brandenburg, D., Antson, A., Dodson, G., and Wollmer, A. (1997) *Biophys. J. 73*, 3287−3298.
21. Rabenstein, M. D., and Shin, Y.-K. (1995) *Proc. Natl. Acad. Sci. U.S.A. 92*, 8239−8243.
22. Langen, R., Oh, K. J., Cascio, D., and Hubbell, W. L. (2000) *Biochemistry 39*, 8396−8405.
23. Hustedt, E. J., Smirnov, A. I., Laub, C. F., Cobb, C. E., and Beth, A. H. (1997) *Biophys. J. 74*, 1881−1887.
24. Mchaourab, H. S., Oh, K. J., Fang, C. J., and Hubbell, W. L. (1997) *Biochemistry 36*, 307−316.
25. Mchaourab, H. S., Lietzow, M. A., Hideg, K., and Hubbell, W. L. (1996) *Biochemistry 35*, 7692−7704.
26. Columbus, L., Kálai, T., Jekõ, J., Hideg, K., and Hubbell, W. L. (2001) *Biochemistry 40*, 3838−3846.
27. Matsumara, M., and Matthews, B. W. (1989) *Science 243*, 792−794.
28. Ho, S. N., Hunt, H. D., Horton, R. M., Pullen, J. K., and Pease, L. R. (1989) *Gene 7*, 51−59.
29. Sauer, U. H., Dao-pin, S., and Matthews, B. W. (1992) *J. Biol. Chem. 267*, 2393−2399.
30. Hankovsky, H. O., Hideg, K., and Lex, L. (1980) *Synthesis*, 914−916.
31. Berliner, L. J., Grunwald, J., Hankovsky, H. O., and Hideg, K. (1982) *Anal. Biochem. 119*, 450−453.
32. Kálai, T., Balog, M., Jekõ, J., and Hideg, K. (1998) *Synthesis 10*, 1476−1482.
33. Hubbell, W. L., Froncisz, W., and Hyde, J. H. (1987) *Rev. Sci. Instrum. 58*, 1879−1886.
34. Mchaourab, H. S., Kálai, T., Hideg, K., and Hubbell, W. L. (1999) *Biochemistry 38*, 2947−2955.
35. Pake, G. E. (1948) *J. Chem. Phys. 16*, 327−336.

BI011544W